Outage Probability in RIS-assisted LoRa Networks with Hardware Impairments and Asymmetric Channels

Lam-Thanh Tu[1], Bui Vu Minh[2], and Tan N. Nguyen[1]

[1]*Ton Duc Thang University, Ho Chi Minh City, Vietnam,*
[2]*Nguyen Tat Thanh University, Ho Chi Minh City, Vietnam*

https://doi.org/10.26636/jtit.2026.1.2315

Abstract — This paper investigates the performance of reconfigurable intelligent surface (RIS)-assisted LoRa networks. Specifically, we consider a LoRa system enhanced by RIS under the influence of hardware impairments and asymmetric channel conditions. A closed-form expression for the outage probability at end devices is derived using the method of moments. The accuracy of the proposed analytical framework is extensively validated through Monte Carlo simulations. Several important insights are drawn from both the theoretical analysis and simulation results. In particular, the system's performance is significantly enhanced by an increase in the number of RIS elements and the transmission power of the gateway. Furthermore, comparisons with related works described in the literature are made to show that the proposed system outperforms these existing approaches simply by increasing the number of RIS elements. Additionally, we reveal that a higher spreading factor (SF) does not necessarily lead to worse performance than a lower SF, and the impact of hardware impairments is found to be minor under typical operating conditions.

Keywords — asymmetric channels, hardware impairments, long range, outage probability, reconfigurable intelligent surfaces

1. Introduction

LoRa networks have significantly improved the Internet of Things (IoT) by allowing long-range communication between devices while maintaining low energy consumption [1]. Using a distinctive modulation technique, LoRa ensures robust signal quality and reduced interference, supporting communication distances of up to 15 km in rural areas and 2 to 5 km in urban environments. Its low data rate makes it ideal for applications such as smart agriculture, environmental monitoring, and asset tracking.

One of LoRa's key advantages is its high energy efficiency (EE), allowing devices to operate for up to ten years on a single battery, making it suitable for large-scale IoT deployments. The architecture of LoRa networks is simple and scalable, with end devices transmitting data to gateways which then forward the information to a centralized server. This design eases the coordination of numerous devices, while the LoRa WAN protocol ensures secure and reliable communication through mechanisms such as adaptive data rate control and data encryption.

In comparison, other low-power wide area network (LPWAN) technologies such as NB-IoT [2] and Sigfox also aim to deliver energy-efficient wide area coverage, but LoRa distinguishes itself through its license-free spectrum use and flexible network deployment. As the IoT landscape continues to expand, LoRa remains a critical enabler of smart city initiatives and industrial automation, by offering a compelling blend of long-range connectivity and ultra-low power operation.

Reconfigurable intelligent surfaces (RIS) represent an emerging innovation in wireless communication, capable of actively shaping electromagnetic waves to improve signal transmission [3]. Composed of inexpensive components, RIS can manipulate signal properties such as phase, amplitude, and polarization to address issues such as signal degradation and interference. This leads to stronger and more widespread coverage without the need for additional transmitters. RIS has great potential for future networks, IoT systems, and smart city infrastructure, where connectivity is paramount.

By integrating RIS with LoRa networks, the performance of low-power IoT systems can be improved. RIS can help guide LoRa signals around physical barriers, enhancing signal integrity, and reducing data loss. This results in more reliable communication over extended distances. Since RIS operates passively, it complements LoRa's low-energy design, increasing network capacity without increasing power demands. The combination of LoRa and RIS supports more densely populated IoT environments and strengthens connectivity for applications such as precision agriculture, environmental sensing, and industrial automation.

Although LoRa networks operate at sub-GHz frequencies that inherently exhibit favorable propagation and penetration characteristics, their performance can still degrade in practical scenarios involving dense urban environments, shadowing, or deep fading. Furthermore, the low transmit power and the simple modulation scheme limit LoRa's ability to maintain reliable communication with distant or indoor-installed end devices. To overcome these limitations, integrating RIS into LoRa networks offers an efficient and cost-effective enhancement. Owing to their ability to reconfigure the wireless propagation environment by intelligently adjusting the phase of the reflected signals, RIS is capable of strengthening the

received power and mitigating the effects of non-linear sight (NLOS) conditions without introducing additional active components or power consumption [3]. Consequently, the joint use of LoRa and RIS combines the long-range, low-power benefits of LoRa with the passive beamforming and coverage-improving capabilities of RIS, resulting in more reliable connectivity, improved outage performance, and extended communication range for large-scale IoT deployments.

2. Related Work

Several problems involving LoRa networks were studied in [4]–[14]. More precisely, the work presented in [4] proposed a novel modulation scheme based on a single bit space-time block code. Based on the proposed modulation scheme, the bit error rate (BER) is significantly reduced. On the other hand, the authors of [5] minimized power consumption while satisfying the quality of service by considering hybrid systems that include both grid-based and renewable energy sources. The problem is solved by deploying the reinforcement learning approach.

The work described in [6] also relied upon deep learning to address coverage probability (Pcov) performance in a scenario in which many power beacons are used to wirelessly charge the battery of end devices (EDs), while the double training approach was proposed in [7] to estimate the energy efficiency (EE) of LoRa networks. The authors of [8] proposed an approach to allow EDs to estimate and compensate for the Doppler shift before transmitting information to low-Earth orbit (LEO) satellites.

On the other hand, the EE of LoRa networks that took into account all states and their associated power consumption levels of the EDs were investigated in [10]. The slotted ALOHA access protocol and carrier-sense multiple access protocol (CSMA) were proposed and studied in [11]. The authors showed that the slotted ALOHA protocol outperformed its pure ALOHA and CSMA counterparts.

The Pcov of the LoRa networks enabled by energy harvesting (EH) was derived in [12] based on nonlinear EH modelling. The authors in [13] derived the Pcov of LoRa networks employing either antenna diversity (using multiple antennas at the gateway) or time diversity. They demonstrated that utilizing diversity techniques is beneficial for system performance. However, their analysis focused solely on uplink LoRa networks and assumed the absence of hardware impairments at both the transmitter and receiver. In practice, this assumption is difficult to satisfy, especially when many antennas are deployed.

On the other hand, the authors in [14] investigated the performance of LoRa dual hop uplink relay networks. Their results showed that shortening the transmission distance can improve Pcov. However, this work did not address how synchronization is achieved among the gateway, EDs, and relays. Furthermore, the impact of asymmetric channels was not considered.

Regarding RIS-assisted wireless systems, the authors of [15] simultaneously optimized the non-orthogonal multiple access (NOMA) transmit power of a LEO satellite and the passive beamforming of RIS, assuming imperfect successive interference cancelation for the NOMA-satellite communications. The work presented in [16] derived the outage probability (OP) of NOMA systems with asymmetric channels comprising $\eta - \mu$ and Rayleigh fading channels. In [17] the latency to perform RIS communications systems aided by tasks of all users in the mobile edge computing (UAV). A combination of localization and communications in integrated sensing and communication (ISAC) systems assisted by RIS was proposed in [18]. The authors minimized the squared position error bound taking into consideration the transmit beamforming vector, phase shift of the RIS elements, and subcarrier assignments.

The trade-off between the security and reliability of RIS-assisted multi-hop cooperative communications with fountain codes was investigated in [19]. The derivations of OP, ergodic capacity, and EE of the cognitive radio NOMA network were provided in [20]. On the other hand, the performance of the two-way RIS-aided systems was studied in [21], under both optimal and random phase shift designs.

In [22], the authors investigated the impact of hardware impairment (HI) on the spectral efficiency (SE) of massive multiple-input multiple-output (MIMO) over Rician fading distributions. Meanwhile, paper [23] examined the performance of cognitive NOMA systems under hardware impairments and two user selection strategies, namely path-loss-based and channel gain-based selection. Their findings show that neither scheme consistently outperforms the other in all operating conditions. This suggests that an adaptive user selection mechanism, capable of switching between strategies based on network state, would be more effective in optimizing overall system performance.

The work described in [24] studied the location of RIS-aided systems under the influence of HI, while the performance analysis of rateless codes-based communication with transmit antenna selection, the harvest-to-jam technique, and hardware impairments was investigated in [25]. A similar work is presented in [26], where the authors analyze a LoRa system employing a single RIS to enhance the gateway-to-end-device link under favorable line of sight conditions. Their findings show that properly configured RIS phase shifts can substantially extend LoRa coverage.

This work advances the analysis in several important aspects: we explicitly incorporate transmitter and receiver hardware impairments, account for phase noise at the RIS, consider asymmetric fading conditions (Rician for the gateway-RIS link and Rayleigh for both the RIS-ED and direct links), and derive closed-form OP expressions under these practical impairments. While [26] assumes ideal RIS control and perfect hardware, our model includes both finite phase-shift resolution and RIS hardware imperfections. Consequently, the proposed framework significantly broadens the scope of [26] and offers a performance analysis that better reflects real-world IoT/LPWAN deployments.

The main contributions and novelties of the present work are primarily summarized as follows:

- Asymmetric systems in RIS-aided LoRa networks are considered, where the fading subject to the first-hop gateway to RIS is different from the second hop. Furthermore, we also consider the direct link from the gateway to the emergency department and study the impact of hardware impairments at both the transmitter and the receiver.
- A closed-form expression for OP is derived using the moment method (MM), which remains accurate for an arbitrary number of RIS elements, unlike approaches based on the central limit theorem (CLT) which typically require many RIS elements to be valid.
- We highlight several key insights from the simulation results. Specifically, we observe that an increase in the number of RIS elements and the transmit power of the gateway significantly improves OP. Additionally, we find that a larger SF does not necessarily lead to worse OP performance and that this relationship is more nuanced. Finally, the impact of hardware impairments on the overall performance of the system in LoRa networks that are considered RIS-assisted is shown to be minor.

The structure of the paper is organized as follows: Section 3 describes the system model, while its performance is analyzed in Section 4. Section 5 presents numerical calculations and discussions. Finally, Section 6 concludes the article. Table 1 summarizes the abbreviations used.

Tab. 1. List of acronyms used throughout the paper.

Acronym	Definition
AN	Artificial noise
AWGN	Additive white Gaussian noise
CLT	Central limit theorem
CSI	Channel state information
EE	Energy efficiency
ED	End device
HI	Hardware impairment
IoT	Internet of Things
LPWAN	Low power wide area network
LoRa	Long range
LOS / NLOS	Line-of-sight / non-line-of-sight
MM	Moment method
NOMA	Non-orthogonal multiple access
OP	Outage probability
RIS	Reconfigurable intelligent surface
SF	Spreading factor
SNR	Signal-to-noise ratio
STAR-RIS	Simultaneous transmitting and reflecting RIS
Tx / Rx	Transmitter / receiver
UAV	Unmanned aerial vehicle

3. System Model

Let us consider a downlink of single gateway LoRa networks as shown in Fig. 1. The gateway is located at the center of the disk with radius P, while EDs are randomly distributed around the gateway. The considered networks also comprise a RIS with K elements, in order to help the gateway send downlink information to the EDs. We assume that all nodes in the networks are equipped with a single antenna. The entire transmission takes place in one time slot.

3.1. Channel Modeling

All transmission links in the systems are subjected to both small-scale fading and large-scale path loss and are modeled in the sequel.

Small-scale fading is modeled by Rician and Rayleigh distributions. In particular, the channel coefficient from the gateway to the RIS will be modeled as a Rician distribution, and the link from the RIS to the EDs will follow a Rayleigh distribution. On the other hand, the direct link from the gateway to the ED always follows the Rayleigh distribution.

Path-loss is modeled based on the popular unbounded path-loss model and is formulated as [27]:

$$O_{x,y} = O_0 \, d_{x,y}^{\chi_a} \, , \tag{1}$$

where $d_{x,y}$ denotes the transmission distance from the transmitter to the receiver and χ_a with $a \in \{L, N\}$ represents the path-loss exponent.

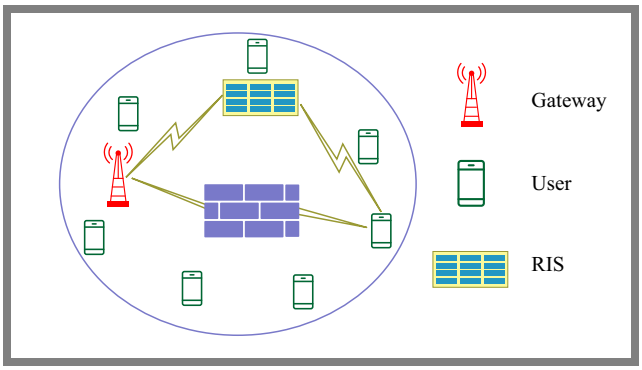

Fig. 1. RIS-aided downlink LoRa networks under consideration.

In this work, we consider different path loss exponents for different links. Specifically, the links from the gateway to the ED and from the RIS to the EDs are subject to Rayleigh fading and therefore experience a higher path loss exponent, denoted by χ_N. On the contrary, the link from the gateway to the RIS follows a Rician distribution and enjoys a lower path loss exponent χ_L. The term O_0 is the path loss constant measured at a reference distance of 1 m and depends on the carrier frequency given by:

$$O_0 = \left(\frac{4\pi f_c}{c}\right)^2 \, ,$$

where f_c is the carrier frequency and c is the speed of light.

3.2. Characteristics of Rayleigh and Rician Distributions

Since Rayleigh fading is a special case of the Rician distribution, we focus on the Rician case and highlight the Rayleigh case as a specific instance. Let C denote the ratio of the power in the LOS component to the power in all NLOS components, and let L represent the total power, including both LOS and NLOS paths. The mean and variance of a random variable (RV) X following the Rician distribution are calculated as follows [28]:

$$\begin{aligned} \mathbb{E}\{X\} &= \sqrt{\frac{\pi L}{4(C+1)}} e^{\frac{-C}{2}} \left[(1+C) I_0 \frac{C}{2} + C I_1 \frac{C}{2}\right], \\ \mathrm{Var}\{X\} &= L - \mu_X^2 \end{aligned} \quad (2)$$

where $I_n(\cdot)$ denotes the modified Bessel function of the first kind of order n. It is obvious that when $C = 0$, the distribution reduces to the Rayleigh distribution. The operators $\mathbb{E}\{\cdot\}$ and $\mathrm{Var}\{\cdot\}$ represent the expectation and the variance, respectively.

3.3. Spreading Factor Allocation

In this paper, the conventional distance-based SF assignment scheme is adopted to assign SFs to EDs. Specifically, an ED is assigned the o-th SF, $o \in \{7, \ldots, 12\}$, if its transmission distance to the gateway falls within the following range:

$$\left[\frac{(o-7)P}{6}, \frac{(o-6)P}{6}\right) .$$

3.4. Asymmetric Channels

In many wireless communication systems, especially in multi-hop scenarios, assuming a uniform fading distribution across all hops often oversimplifies the complex nature of real-world propagation environments. A more realistic and insightful approach is to consider scenarios where each hop experiences a distinct fading distribution.

This is motivated by the fact that the physical path and surrounding environment of each link can vary significantly. For example, the first hop may benefit from a clear LOS path in an open suburban area, resulting in Rician fading, while a subsequent hop might traverse a densely cluttered urban environment, leading to severe Rayleigh fading.

Accordingly, this paper adopts an asymmetric fading model. Wireless links in the LoRa network are modeled using a combination of Rician and Rayleigh fading. Specifically, the gateway-to-RIS link follows a Rician distribution to represent a scenario with a strong LOS component, as the RIS is typically placed at elevated or strategically selected positions with clear visibility of the gateway.

On the contrary, both the RIS-to-ED and the direct gateway-to-ED links experience Rayleigh fading, representing NLOS conditions caused by scattering and shadowing in practical IoT deployments [29]. It is worth emphasizing that the proposed analytical framework is general and can be directly applied to the reverse scenario (i.e., Rician fading for the RIS-to-ED link and Rayleigh fading for the gateway-to-RIS link) without modification.

3.5. Hardware Impairments

Although much of the existing research assumes ideal conditions for transmitter and receiver hardware, this study adopts a more practical perspective by considering the inevitable effects of hardware imperfections at both ends of the communication system. This consideration is especially important for setups involving affordable technologies such as LoRa, where flawless hardware is an unrealistic assumption.

More precisely, both the gateway and EDs are assumed to employ low-cost transceiver hardware, consistent with LoRa technology. The residual distortions introduced by non-ideal mixers, amplifiers, and oscillators are modeled as additive Gaussian hardware impairment noise [30], denoted as Ξ_X and Ξ_Y , parameterized by zero mean as well as variances $\delta^2_{\Xi_G}$ and $\delta^2_{\Xi_o}$. This modeling approach is widely used and accurately reflects low-cost IoT transceivers [31].

3.6. RIS Phase Modeling

The proposed model also accounts for non-idealities introduced by the RIS itself. Unlike many existing studies that assume perfectly tunable, continuous phase adjustments, we adopt a more practical representation in which each RIS element operates with quantized phase control.

Let $\mathcal{Q}$ be the number of quantization bits assigned to each element. Under this assumption, the resulting phase perturbation θ is modeled as a uniformly distributed random variable throughout the interval:

$$\left[-2^{-\mathcal{Q}}\pi,\, 2^{-\mathcal{Q}}\pi\right] ,$$

reflecting the inherent discretization error.

It is worth noting that the adopted phase-shift model is well supported by recent studies on programmable metasurfaces, showing that even low-cost RIS implementations with only a few quantization bits can achieve near-continuous phase control at sub-GHz and microwave frequencies [32], [33]. Furthermore, as illustrated in Tab. 2, RIS configurations employing only 2–3 bits of phase resolution can maintain more than 90% of the performance of an ideal continuous phase RIS, particularly in the low-frequency bands characteristic of LoRa systems.

These observations indicate that the aggregate reflection gain of the RIS effectively compensates for quantization-induced errors, thereby confirming that the adopted phase-shift model is both practically realistic and analytically tractable for modern metasurface hardware.

3.7. Signal-to-Noise Ratios at EDs

The received signal of a typical ED utilizing o-th SF is formulated as [34]:

$$\begin{aligned} y_o =& \sqrt{B_G}\left[\sqrt{O^{-1}_{G,o}} h_{G,o} + \sqrt{O^{-1}_{G,R} O^{-1}_{R,o}} \sum_{k=1}^{K} h_{G,k} \Phi_k h_{k,o}\right] \\ & \times (t_G + \Xi_G) + \Xi_o + n_o , \end{aligned} \quad (3)$$

where BG denotes the transmit power of the gateway, $O_{G,o}$, $O_{R,G}$, and $O_{R,o}$ represent the large-scale path-loss from the gateway to the ED using the o-th SF, from the gateway to the RIS, and from the RIS to the ED with o-th SF, respectively.

The t_G is the transmit signal of the gateway, while Ξ_G and Ξ_o denote the HI at the gateway and the ED, respectively. n_o is the additive white Gaussian noise (AWGN) at the receiver. The channel coefficients are represented by $h_{G,o}$ (gateway to the ED using SF o), $h_{G,k}$ (gateway to the k-th element of the RIS), and $h_{k,o}$ (from the k-th RIS element to the ED using SF o).

The phase-shift matrix of the RIS is given by $\Phi = \text{diag}\left(e^{j\iota_1}, \ldots, e^{j\iota_K}\right)$, where $\iota_k \in [-\pi, \pi]$ is the phase shift of the k-th RIS element, and $\text{diag}(\cdot)$ denotes a diagonal matrix.

From Eq. (3), the SINR of the ED using the o-th SF, denoted by ω_o, is given by Eq. (4):

$$\omega_o = \frac{\left|\sqrt{B_G}\left[\sqrt{O_{G,o}^{-1}}h_{G,o} + \sqrt{O_{G,R}^{-1}O_{R,o}^{-1}}\sum_{k=1}^{K} h_{G,k}\Phi_k h_{k,o}\right]\right|^2}{\left|\sqrt{B_G}\left[\sqrt{O_{G,o}^{-1}}h_{G,o} + \sqrt{O_{G,R}^{-1}O_{R,o}^{-1}}\sum_{k=1}^{K} h_{G,k}\Phi_k h_{k,o}\right]\right|^2 \left(\delta_{\Xi_G}^2 + \delta_{\Xi_o}^2\right) + \sigma_o^2} = \frac{B_G Z^2}{B_G\left(\delta_{\Xi_G}^2 + \delta_{\Xi_o}^2\right) Z^2 + \sigma_o^2}\,. \tag{4}$$

The composite signal term Z is defined as:

$$Z = \left|\sqrt{O_{G,o}^{-1}}\,h_{G,o} + \sqrt{O_{G,R}^{-1}O_{R,o}^{-1}}\sum_{k=1}^{K} h_{G,k}\Phi_k h_{k,o}\right|\,.$$

$$Z = \sqrt{O_{G,o}^{-1}}\,|h_{G,o}| + \sqrt{O_{G,R}^{-1}O_{R,o}^{-1}}\sum_{k=1}^{K} |h_{G,k}|\,|h_{k,o}|\,e^{j\theta_k}\,,$$

where $e^{j\theta_k}$ is the phase error of the k-th element, σ_o^2 is the variance of the AWGN in the ED using o-th SF.

3.8. Performance Metrics

In this paper, OP is considered the main metric to measure the performance of the considered networks. OP of the o-th SF is defined as:

$$\text{OP}_o = \Pr\{\omega_o < \beta_o\} \tag{5}$$

where $\Pr\{\cdot\}$ is the probability operator, β_o denotes the target SINR threshold for the o-th SF and is treated as a constant. The values are given by $\beta = \{-6, -9, -12, -15, -17, -20\}$ dBm, corresponding to SF7 through SF12, respectively. For example, $\beta_7 = -6$ dBm for SF7, and $\beta_{12} = -20$ dBm for SF12.

4. Performance Analysis

The OP of ED used o-th SF is computed as follows:

$$\begin{aligned}\text{OP}_o =& F_Z\sqrt{\frac{\beta_o}{\Psi\left(1-\beta_o\delta^2\right)}}\,U\left(1-\beta_o\delta^2\right)\\ &+ U\left(\beta_o\delta^2 - 1\right)\,,\end{aligned} \tag{6}$$

where $U(\cdot)$ denotes the unit step function, $\delta^2 = \delta_{\Xi_G}^2 + \delta_{\Xi_o}^2$ represents the total HI variance from both the gateway and the ED, $\Psi = \frac{B_G}{\sigma_o^2}$ denotes the average transmit power-to-noise ratio. Additionally, $F_X(x)$ is the cumulative distribution function (CDF) of the random variable X.

Proof. Let us begin the proof by rewriting the definition of the OP in Eq. (5) as follows:

$$\begin{aligned}\text{OP}_o &= \Pr\left\{\omega_o = \frac{B_G Z^2}{B_G\left(\delta_{\Xi_G}^2 + \delta_{\Xi_o}^2\right) Z^2 + \sigma_o^2} < \beta_o\right\}\\ &\overset{(a)}{=} \Pr\left\{Z^2 < \frac{\beta_o}{\Psi\left(1-\beta_o\delta^2\right)}\right\} U\left(1-\beta_o\delta^2\right) + U\left(\beta_o\delta^2 - 1\right)\,.\end{aligned} \tag{7}$$

Here (a) is held by applying the definition of the CDF of a RV and we close the proof. □

By directly inspecting Eq. (6), we observe that if $\beta_o\delta^2 > 1$, the system will always experience an outage. Further analysis reveals that if the negative impact of HI, whether at the transmitter or receiver, is too severe (i.e., when δ^2 is large), the system remains in outage regardless of other system parameters. This leads to the first and most important insight – hardware impairments must be minimized as much as possible to ensure system performance.

Equation (6) also reveals that increasing Ψ is always beneficial for reducing OP, provided that HI remain within acceptable limits-specifically, the condition $\beta_o\delta^2 < 1$ must be satisfied. This indicates that enhanced system performance can be achieved by increasing the transmit power of the gateway or by reducing the noise power, for example, through bandwidth reduction.

Equation (6) also indicates that the closed-form expression of the OP in both considered cases reduces to the CDF of the RV Z.

In the following, we derive the CDF of:

$$Z = \sqrt{O_{G,o}^{-1}}\,|h_{G,o}| + \sqrt{O_{G,R}^{-1}O_{R,o}^{-1}}\sum_{k=1}^{K} |h_{G,k}|\,|h_{k,o}|\,e^{j\theta_k}\,,$$

by applying the method of moments. It should be emphasized that a closed-form expression for the distribution of Z is not available, even under simple fading conditions, such as Rayleigh fading, due to the complexity introduced by the sum of products of multiple random variables. Consequently, prior work in the literature often resorted to using the central

limit theorem to approximate Z as a Gaussian random variable. However, this approach requires a large number of RIS elements to achieve an accurate approximation.

In contrast, the method of moments offers a more accurate and flexible alternative, as it does not rely on the assumption of a large number of RIS elements. Therefore, in this work, we adopt the MM approach and the resulting expression is provided in Theorem 1.

Theorem 1. Let us denote $\widehat{Z}$ is the equivalent RV of Z which follows a gamma distribution with shape and scale parameters denoted as λ and ξ as given below:

$$\lambda = \frac{\left(\mathbb{E}\left\{Z\right\}\right)^2}{\mathrm{Var}\left\{Z\right\}}, \quad \xi = \frac{\mathrm{Var}\left\{Z\right\}}{\mathbb{E}\left\{Z\right\}}, \tag{8}$$

The mean and variance of Z are computed as follows:

$$\begin{aligned}
\mathbb{E}\left\{Z\right\} &= \sqrt{O_{G,o}^{-1}}\mathbb{E}\left\{|h_{G,o}|\right\} \\
&\quad + K\sqrt{O_{G,R}^{-1}O_{R,o}^{-1}}\mathbb{E}\left\{|h_{G,R}|\right\} \\
&\quad \times \mathbb{E}\left\{|h_{R,o}|\right\}\mathbb{E}\left\{e^{j\theta_k}\right\} \\
\mathrm{Var}\left\{Z\right\} &= O_{G,o}^{-1}\mathrm{Var}\left\{|h_{G,o}|\right\} \\
&\quad + KO_{G,R}^{-1}O_{R,o}^{-1}\mathrm{Var}\left\{\mathcal{A}e^{j\theta_k}\right\} \\
\mathrm{Var}\{\mathcal{A} = |\mathrm{h_{G,R}}||h_{R,o}|\} &= (\mathbb{E}\{|h_{G,R}|\})^2\mathrm{Var}\{|\mathrm{h_{R,o}}|\} \\
&\quad + \left(\mathbb{E}\left\{|h_{R,o}|\right\}\right)^2\mathrm{Var}\left\{|h_{G,R}|\right\} \\
&\quad + \mathrm{Var}\left\{|h_{G,R}|\right\}\mathrm{Var}\left\{|h_{R,o}|\right\} \\
\mathrm{Var}\left\{\mathcal{A}e^{j\theta_k}\right\} &= (\mathbb{E}\{\mathcal{A}\})^2\mathrm{Var}\left\{e^{j\theta_k}\right\} \\
&\quad + \mathbb{E}\left(\left\{e^{j\theta_k}\right\}\right)^2\mathrm{Var}\left\{\mathcal{A}\right\} \\
&\quad + \mathrm{Var}\left\{\mathcal{A}\right\}\mathrm{Var}\left\{e^{j\theta_k}\right\}.
\end{aligned} \tag{9}$$

Proof. The proof of (9) is given as follows:

$$\begin{aligned}
&\mathbb{E}\left\{Z\right\} = \sqrt{O_{G,o}^{-1}}\mathbb{E}\left\{|h_{G,o}|\right\} + \sqrt{O_{G,R}^{-1}O_{R,o}^{-1}} \\
&\times \mathbb{E}\left\{\sum_{k=1}^{K}|h_{G,R}|\,|h_{R,o}|\,e^{j\theta_k}\right\} \\
&\overset{(a)}{=} \sqrt{O_{G,o}^{-1}}\mathbb{E}\left\{|h_{G,o}|\right\} \\
&+ K\sqrt{O_{G,R}^{-1}O_{R,o}^{-1}}\mathbb{E}\left\{|h_{G,R}|\,|h_{R,o}|e^{j\theta_k}\right\} \\
&\overset{(b)}{=} \sqrt{O_{G,o}^{-1}}\mathbb{E}\left\{|h_{G,o}|\right\} + K\sqrt{O_{G,R}^{-1}O_{R,o}^{-1}}\mathbb{E}\left\{|h_{G,R}|\right\} \\
&\times \mathbb{E}\left\{|h_{R,o}|\right\}\mathbb{E}\left\{e^{j\theta_k}\right\}, \\
&\mathrm{Var}\left\{Z\right\} = O_{G,o}^{-1}\mathrm{Var}\left\{|h_{G,o}|\right\} + O_{G,R}^{-1}O_{R,o}^{-1} \\
&\times \mathrm{Var}\left\{\sum_{k=1}^{K}|h_{G,k}|\,|h_{k,o}|\,e^{j\theta_k}\right\} \\
&\overset{(c)}{=} O_{G,o}^{-1}\mathrm{Var}\left\{|h_{G,o}|\right\} + KO_{G,R}^{-1}O_{R,o}^{-1}\mathrm{Var}\left\{\mathcal{A}e^{j\theta_k}\right\}.
\end{aligned} \tag{10}$$

where (a), (b) and (c) are attained owing to the independence between direct link and indirect links. Between the first and second hops of the indirect link, we finish the proof.

Tab. 2. Simulation parameters used in the performance evaluation.

Parameter	Symbol/value	Description
Carrier frequency	$f_c = 433$ MHz	LoRa operating frequency
Bandwidth	BW $= 125$ kHz	Transmission bandwidth
Transmit power	$B_G = 4$ dBm	Gateway transmit power
Network radius	$P = 2 - 6$ km	LoRa coverage area
RIS elements	$K = 24 - 80$	Number of reflecting units
Rician factor	$C_{G,R} = 0 - 10$	Gateway to RIS channel condition
Path-loss exponent	$\chi_{\mathrm{LOS}} = 2.2$, $\chi_{\mathrm{NLOS}} = 3.8$	Large-scale fading
HI variance	$\delta_{\Xi_G} = \delta_{\Xi_o} \in [0, 0.5]$	Hardware impairment level
Noise variance	σ_o^2	AWGN at ED
Quantization bits	$\mathcal{Q} = 6$ bits	RIS phase resolution

The mean and variance of the phase error can be found in [35], where the l-th moment is given by $\mathbb{E}\left\{e^{jl\theta_k}\right\} = \mathrm{sinc}\left(2^{-\mathcal{Q}+l-1}\right),\ \forall k.$ □

Finally from Theorem 1 and Eq. (2), we obtain the closed-form expression of the OP:

$$\begin{aligned}
\mathrm{OP}_o = &\frac{\gamma\left(\lambda, \frac{1}{\xi}\sqrt{\frac{\beta_o}{\Psi\left(1-\beta_o\delta^2\right)}}\right)}{\Gamma\left(\lambda\right)}U\left(1-\beta_o\delta^2\right) \\
&+ U\left(\beta_o\delta^2 - 1\right).
\end{aligned} \tag{11}$$

Here $\Gamma(\cdot)$ and $\gamma(\cdot)$ represent Gamma and lower incomplete Gamma function.

5. Numerical Results

In this section, simulation results based on the Monte Carlo method are presented to validate the accuracy of the derived mathematical framework. Without loss of generality, set of simulation parameters are provided in Tab. 2. Here, the system parameters, i.e. carrier frequency $f_c = 433$ MHz, bandwidth BW $= 125$ kHz, and network radius $P = 2 - 6$ km, follow the standard LoRa physical layer settings recommended by the LoRa Alliance. The Rician factor $C_{G,R}$ is varied from 0 to 10 to capture both weak and strong LOS conditions, while the HI variance $\delta_\Xi \in [0, 0.5]$ is chosen to cover practical non-idealities observed in commercial IoT devices.

Figure 2 illustrates the OP performance versus the number of quantization bits $\mathcal{Q}$ per RIS element. The results confirm an excellent agreement between the derived analytical framework and the Monte Carlo simulations, validating the accuracy of

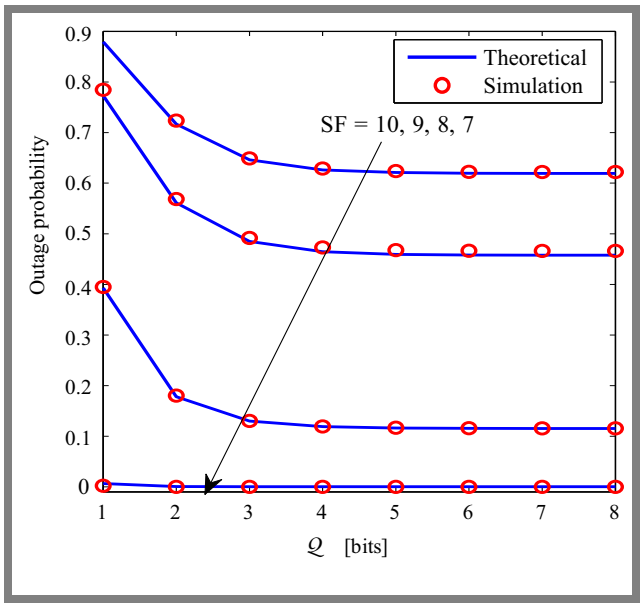

Fig. 2. OP vs. the number of quantization bits $\mathcal{Q}$. Lines are plotted based on Eq. (11), while markers originate from the Monte Carlo simulation.

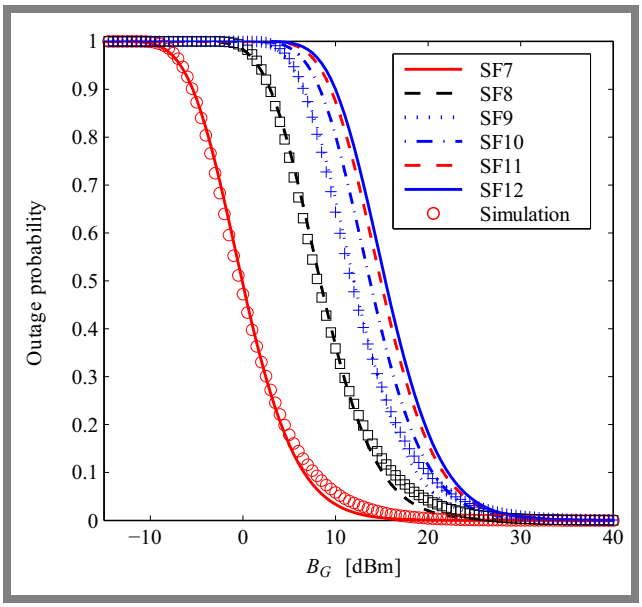

Fig. 3. OP vs. transmit power of gateway B_G. Lines are plotted based on Eq. (11), while markers originate from the Monte Carlo simulation.

the proposed model. It can be observed that increasing the phase resolution improves the OP performance. In particular, the OP decreases significantly when $\mathcal{Q}$ increases from 1 to 2 bits, and then gradually approaches a saturation point for $\mathcal{Q} \geqslant 4$. This indicates that further increasing the RIS phase resolution beyond four bits yields negligible performance improvement. Therefore, without loss of generality, a resolution of $\mathcal{Q} = 6$ bits is adopted in the subsequent analysis.

Figure 3 illustrates the outage performance as a function of the gateway transmit power B_G. It can be observed that the OP decreases monotonically with increasing B_G. Furthermore, smaller SFs generally result in better outage performance, except for SF12, which outperforms SF11. This is because, although SF12 suffers from longer transmission durations, it requires a lower target data rate, leading to a reduced outage probability. Nonetheless, the performance gap among the higher SFs (e.g., SF11 and SF12) is relatively small compared to the gap between these and SF7. The figure also validates the accuracy of the proposed MM-based analytical framework, as the curves generated from the analysis closely match those obtained from Monte Carlo simulations.

The impact of the HI level at both the gateway and EDs on the OP is illustrated in Fig. 4. It is observed that an increase in the HI level δ_Ξ leads to a degradation in OP performance. However, this adverse effect is relatively minor. For instance, with SF8, increasing δ_Ξ from 0 to 0.5 results in a rise in OP from 0.1 to 0.16, which is the largest increase observed among all SFs. Once again, we observe a strong agreement between the simulation results and the proposed analytical framework.

Figure 5 illustrates the OP performance with respect to the number of RIS elements N. It is evident that increasing N significantly enhances the OP performance. Specifically, under the current setup, when $N = 60$, the OP for all SFs approaches 10^{-5} level, and for SF7, this level is achieved even with $N < 30$.

This figure also compares the performance of the proposed network with existing works in the literature. In particular, we compare it with the dual-hop relay-assisted LoRa network in [14] (represented by red curves) and the multiple-antenna gateway scheme in [13] (represented by green – 2 antennas and black curves – 10 antennas). The results show that the proposed framework outperforms these existing approaches by simply increasing the number of RIS elements. It is emphasized that these comparisons are conducted under fair settings. All schemes operate with the same transmit power, experience the same hardware impairments, and are subject to asymmetric channels with identical channel coefficients.

For example, with SF7, the dual hop scheme achieves an OP of 4.2×10^{-6}, while the OPs for the multiple antenna gateway scheme are 0.05 for two antennas and 8×10^{-7} for

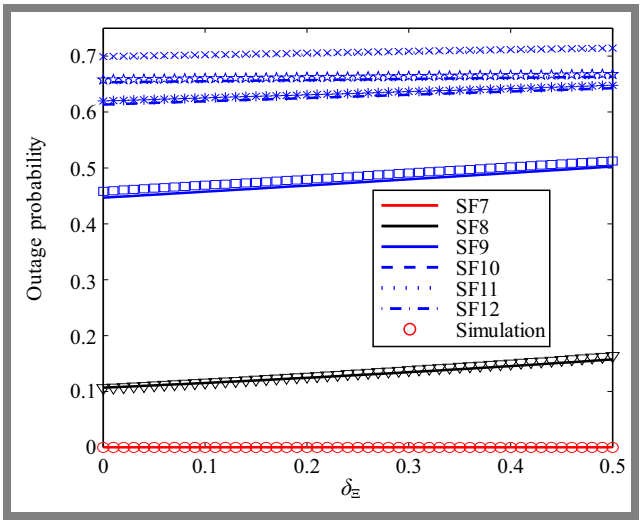

Fig. 4. OP vs. HI level at both the transmitter and receiver $\delta_{\Xi_G} = \delta_{\Xi_D} = \delta_\Xi$. Lines are plotted according to Eq. (11) while markers originate from the Monte Carlo simulation.

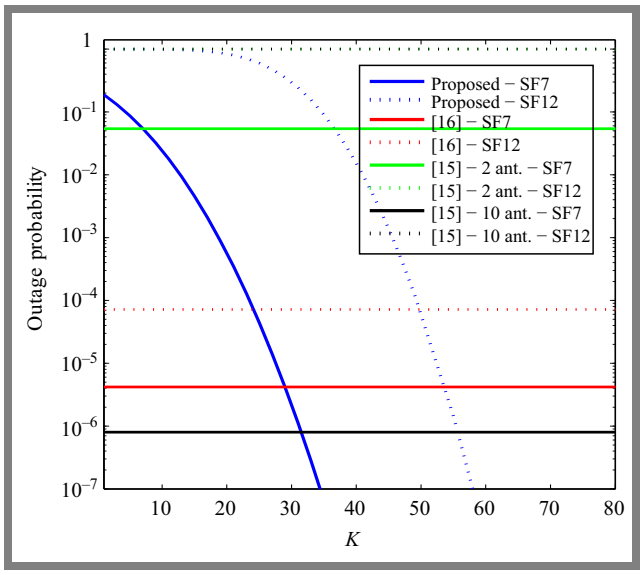

Fig. 5. OP vs. number of RIS elements K. Blue curves are plotted on Eq. (11), red curves originate from [14], while green and black curves originate from [13].

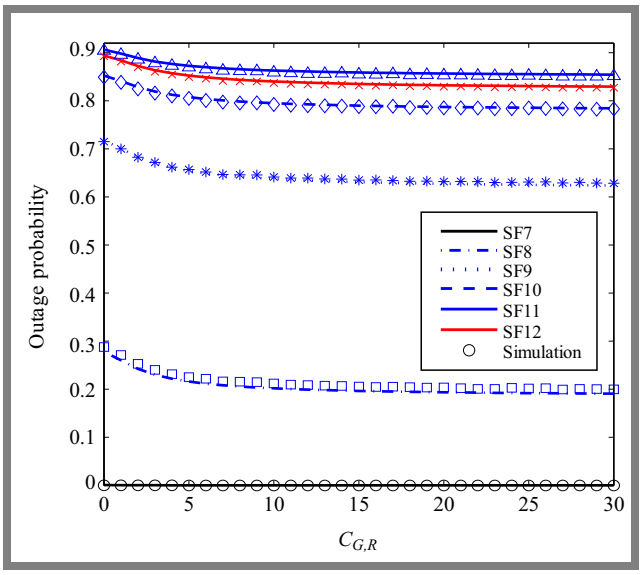

Fig. 6. OP vs. Rician factor of the link from the gateway to the RIS, $C_{G,R}$. Lines are plotted according to Eq. (11), while markers originate from the Monte Carlo simulation.

ten antennas. To match the performance of the 10-antenna configuration, the proposed scheme requires only 31 RIS elements. For SF12, an interesting observation arises: OP performance of both the 2- and 10-antenna configurations in the multiple-antenna gateway scheme is approximately 0.998, indicating poor reliability.

In contrast, the dual-hop scheme achieves an OP of 7.18×10^{-5}, while the proposed RIS-assisted scheme requires 50 elements to achieve comparable performance. In general, these comparisons demonstrate that the proposed scheme not only outperforms existing works described in the literature, but also effectively mitigates the adverse impact of hardware impairments by simply increasing the number of RIS elements.

Figure 6 presents the impact of the Rician factor of the link from the gateway to the RIS, denoted as $C_{G,D}$, on the OP. It is observed that increasing $C_{G,D}$ improves the OP performance. However, this improvement saturates across all SFs. Specifically, the OP decreases rapidly as $C_{G,D}$ increases from 0 to 5, but beyond this point, the rate of improvement diminishes and the OP becomes nearly constant.

The impact of the Rician factor on all links is investigated in Fig. 7, where $C_{G,R} = C_{G,D} = C_{R,D} = C$, indicating a symmetric system setup. Overall, the OP decreases as C increases, which aligns with practical expectations-systems perform better under more favorable channel conditions (i.e., stronger LOS components). The most significant improvement is observed for SF9, where the OP drops from 0.7 to approximately 0.15. Interestingly, the OP for SF12 increases slightly with higher C, which suggests that in this scenario, the lower target rate of SF12 may be offset by other limiting factors as the channel improves.

The OP performance with respect to the network radius P is investigated in Fig. 8. As expected, increasing the network radius degrades system performance. Under the current setup, the OP approaches one for all SFs when $P > 5$ km. To mitigate this performance degradation, one could consider increasing the number of RIS elements and/or the transmit power of the gateway.

It is worth noting that the present work focuses on theoretical modeling and analytical performance evaluation of RIS-assisted LoRa networks under hardware impairments and asymmetric fading conditions.

The objective is to establish a fundamental understanding of the outage behavior and to provide closed-form expressions that can serve as benchmarks for future experimental verification. Although hardware validation and field trials are not included in this study, the analytical and simulation results have been carefully cross-verified and are consistent with re-

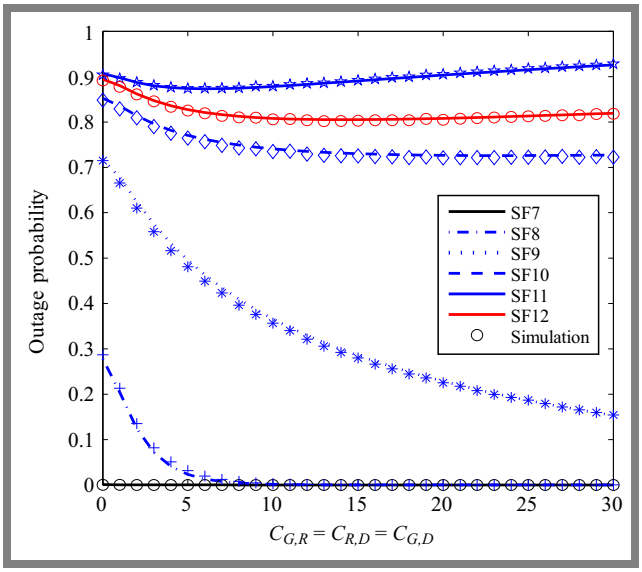

Fig. 7. OP vs. Rician factor of all links, $C_{G,R} = C_{G,D} = C_{R,D}$. Lines are plotted according to Eq. (11), while markers originate from the Monte Carlo simulation.

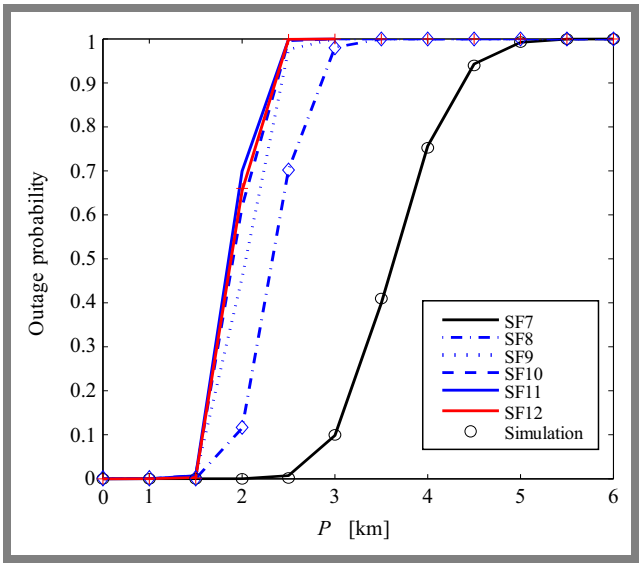

Fig. 8. OP vs. network radius, P. Lines are plotted according to Eq. (11), while markers originate from the Monte Carlo simulation.

cent measurement-based studies of LoRa and RIS systems reported in the literature [32], [33].

Furthermore, parameter values (e.g., carrier frequency, bandwidth, and Rician factors) were selected according to the practical LoRa system specifications and verified through Monte Carlo simulations for accuracy. In future work, we plan to implement a small-scale RIS-aided LoRa prototype using a programmable metasurface and commercial LoRa transceivers (e.g., SX1276) to experimentally validate the analytical framework and further quantify the impact of practical hardware imperfections.

6. Conclusions

This paper investigates the performance of LoRa networks under the impact of hardware impairments. A closed-form expression for the OP is derived using the method of moments. Numerical results reveal several key insights: the OP decreases monotonically with an increase in gateway transmit power, the number of RIS elements, and the Rician factor of the gateway-to-RIS link, among others.

It was emphasized that the analytical framework developed in this paper provides important insights into the performance of RIS-assisted LoRa networks under hardware impairments, phase noise, and asymmetric fading conditions, and several limitations should be acknowledged. The current system model considers a single RIS and a single gateway operating in the downlink direction, assuming quasi-static channels and perfect synchronization. In practical deployments, time-varying channels, interference from multiple gateways, and imperfect synchronization may introduce additional performance degradation. The RIS is modeled as a planar reflective surface with ideal or quantized phase control. Extensions to other reconfigurable architectures such as STAR-RIS or hybrid active-passive RIS could capture more realistic propagation scenarios. The proposed framework focuses on the probability of an outage as the primary metric. Incorporating additional metrics such as energy efficiency, latency, or spectral efficiency would provide a more comprehensive evaluation of the performance of the system.

Furthermore, the adopted mathematical framework is general enough to be extended beyond LoRa networks. By adapting the physical-layer parameters and channel characteristics, the same analytical methodology can be applied to other LPWAN technologies such as NB-IoT and Sigfox, or to short-range IoT protocols such as IEEE 802.15.4. This model can also be integrated with stochastic geometry to evaluate large-scale random deployments or with rate-adaptive mechanisms to capture dynamic data-rate selection in heterogeneous IoT environments. These extensions would further enhance the applicability of the proposed framework and bridge the gap between theoretical modeling and practical IoT network design.

Acknowledgments

This research is funded by Ton Duc Thang University under grant number FOSTECT.2024.21.

References

[1] U. Raza, P. Kulkarni, and M. Sooriyabandara, "Low Power Wide Area Networks: An Overview", *IEEE Communications Surveys & Tutorials*, vol. 19, pp. 85–873, 2017 (https://doi.org/10.1109/COMST.2017.2652320).

[2] B. Doori and A. Zurfi, "Decreasing the RA Collision Impact for Massive NB-IoT in 5G Wireless Networks", *Jordanian Journal of Computers and Information Technology*, vol. 7, pp. 268–277, 2021 (https://doi.org/10.5455/jjcit.71-1620292048).

[3] A. Reda, T. Mekkawy, and A. Mahran, "Towards Optimizing the Downlink Transmit Power in UAV-integrated IRS Wireless Systems", *Jordanian Journal of Computers and Information Technology*, vol. 11, pp. 184–196, 2025 (https://doi.org/10.5455/jjcit.71-1727208249).

[4] H. Zhang *et al.*, "1-bit STBC-LoRa Modulation for Extreme Environment Communications", *IEEE Wireless Communications Letters*, vol. 14, pp. 2094–2098, 2025 (https://doi.org/10.1109/LWC.2025.3563205).

[5] R. Hamdi *et al.*, "LoRa-RL: Deep Reinforcement Learning for Resource Management in Hybrid Energy LoRa Wireless Networks", *IEEE Internet of Things Journal*, vol. 9, pp. 6458–6476, 2022 (https://doi.org/10.1109/JIOT.2021.3110996).

[6] T.T.H. Nguyen *et al.*, "Coverage Probability of EH-enabled LoRa Networks – A Deep Learning Approach", *EAI Endorsed Transactions on Industrial Networks and Intelligent Systems*, vol. 12, art. no. 6780, 2024 (https://doi.org/10.4108/eetinis.v12i2.6780).

[7] L.T. Tu *et al.*, "Energy Efficiency Optimization in LoRa Networks – A Deep Learning Approach", *IEEE Transactions on Intelligent Transportation Systems*, vol. 23, pp. 15435–15447, 2022 (https://doi.org/10.1109/TITS.2022.3183073).

[8] M.A. Ullah *et al.*, "Extending the LoRa Direct-to-satellite Limits: Doppler Shift Pre-compensation", *IEEE Open Journal of the Communications Society*, vol. 6, pp. 2256–2273, 2025 (https://doi.org/10.1109/OJCOMS.2025.3554077).

[9] H.R. Barua and I.A. Chowdhury, "Design and Simulation of a High Performance 5G mm-Wave MIMO Antenna Array for Mobile Applications", *J. of Advanced Engineering and Computation*, vol. 8, art. no. 437, 2024 (https://doi.org/10.55579/jaec.202481.437).

[10] L.T. Tu, A. Bradai, Y. Pousset, and A.I. Aravanis, "Energy Efficiency Analysis of LoRa Networks", *IEEE Wireless Communications Letters*,

vol. 10, pp. 1881–1885, 2021 (https://doi.org/10.1109/LWC.2021.3084996).
[11] L. Beltramelli, A. Mahmood, P. Osterberg, and M. Gidlund, "LoRa Beyond ALOHA: An Investigation of Alternative Random Access Protocols", *IEEE Tran. on Industrial Informatics*, vol. 17, pp. 3544–3554, 2021 (https://doi.org/10.1109/TII.2020.2977046).
[12] T.T. Duy *et al.*, "On the Performance of the Coverage Probability of LoRa Networks with Non-linear Energy Harvesting", *2024 International Conference on Advanced Technologies for Communications (ATC)*, Ho Chi Minh City, Vietnam, 2024 (https://doi.org/10.1109/ATC62344.2024.10908157).
[13] A. Hoeller *et al.*, "Analysis and Performance Optimization of LoRa Networks with Time and Antenna Diversity", *IEEE Access*, vol. 6, pp. 32820–32829, 2018 (https://doi.org/10.1109/ACCESS.2018.2839064).
[14] T.H. Nguyen *et al.*, "Performance Analysis and Optimization of the Coverage Probability in Dual Hop LoRa Networks with Different Fading Channels", *IEEE Access*, vol. 8, pp. 107087–107102, 2020 (https://doi.org/10.1109/ACCESS.2020.3000600).
[15] W.U. Khan *et al.*, "RIS-assisted Energy-efficient LEO Satellite Communications with NOMA", *IEEE Transactions on Green Communications and Networking*, vol. 8, pp. 780–790, 2024 (https://doi.org/10.1109/TGCN.2023.3344102).
[16] I. Khirwar, A. Gupta, B. Verma, and P. Garg, "Asymmetric Dual-hop NOMA Based Communication System with Practical Constraints: Imperfect CSI, HWI and ISIC", *2023 9th International Conference on Signal Processing and Communication (ICSC)*, Noida, India, 2023 (https://doi.org/10.1109/ICSC60394.2023.10441547).
[17] P.Q. Truong *et al.*, "Computation Offloading and Resource Allocation Optimization for Mobile Edge Computing-aided UAV-RIS Communications", *IEEE Access*, vol. 12, pp. 107971–107983, 2024 (https://doi.org/10.1109/ACCESS.2024.3435483).
[18] P. Saikia, K. Singh, W.J. Huang, and T.Q. Duong, "Hybrid Deep Reinforcement Learning for Enhancing Localization and Communication Efficiency in RIS-aided Cooperative ISAC Systems", *IEEE Internet of Things Journal*, vol. 11, pp. 29494–29510, 2024 (https://doi.org/10.1109/JIOT.2024.3411158).
[19] V.T. Ty *et al.*, "Security-reliability Tradeoff of Multi-hop Secure Communication Networks Using Fountain Codes and RIS-aided Cooperative Communication", *2023 International Conference on Advanced Technologies for Communications (ATC)*, Da Nang, Vietnam, 2023 (https://doi.org/10.1109/ATC58710.2023.10318517).
[20] X. Li *et al.*, "Performance Analysis of Star-RIS-CR-NOMA-based Consumer IoT Networks for Resilient Industry 5.0", *IEEE Transactions on Consumer Electronics*, vol. 70, pp. 1380–1391, 2024 (https://doi.org/10.1109/TCE.2023.3319402).
[21] L.T. Tu *et al.*, "Performance of RIS-assisted Two-way Communications with Phase Noise", AETA 2022 – Recent Advances in Electrical Engineering and Related Sciences: Theory and Application, pp. 707–718, 2022 (https://doi.org/10.1007/978-981-99-8703-0_59).
[22] X. Chen *et al.*, "Performance of Cell-free Massive MIMO Systems with Channel Aging and Phase Noise Over Rician Fading Channels", *IEEE Transactions on Vehicular Technology*, vol. 74, pp. 17765–17778, 2025 (https://doi.org/10.1109/TVT.2025.3581908).
[23] L.T. Tu, V.N.Q. Bao, and B. An, "On the Performance of Outage Probability in Underlay Cognitive Radio with Imperfect CSI", *2013 International Conference on Advanced Technologies for Communications (ATC 2013)*, Ho Chi Minh City, Vietnam, 2013 (https://doi.org/10.1109/ATC.2013.6698091).
[24] X. Zhang, N.P. Le, and M.S. Alouini, "RIS-based DOA Estimation for Communication-assisted Sensing Systems Under Hardware Impairments", *IEEE Open Journal of Vehicular Technology*, vol. 6, pp. 1736–1748, 2025 (https://doi.org/10.1109/OJVT.2025.3580041).
[25] P.T. Tin *et al.*, "Rateless Codes-based Secure Communication Employing Transmit Antenna Selection and Harvest-to-jam Under Joint Effect of Interference and Hardware Impairments", *Entropy*, vol. 21, art. no. 700, 2019 (https://doi.org/10.3390/e21070700).
[26] X. Zhang *et al.*, "A New Reconfigurable Intelligent-surface-assisted LoRa System", *IEEE Transactions on Vehicular Technology*, vol. 71, pp. 9055–9060, 2022 (https://doi.org/10.1109/TVT.2022.3173675).
[27] S.P. Le *et al.*, "On the Secrecy Performance of Reconfigurable Intelligent Surfaces-assisted Satellite Networks Under Shadow-Rician Channels", *IEEE Transactions on Aerospace and Electronic Systems*, vol. 61, pp. 6794–6808, 2025 (https://doi.org/10.1109/TAES.2025.3532227).
[28] M.K. Simon and M.S. Alouini, *Digital Communication over Fading Channels*, Wiley, Newark, 900 p., 2005 (https://doi.org/10.1002/0471715220).
[29] J. Breitegger *et al.*, "Long-term LoRa Experiments in a Chemical Plant", *2021 22nd IEEE International Conference on Industrial Technology (ICIT)*, Valencia, Spain, 2021 (https://doi.org/10.1109/ICIT46573.2021.9453474).
[30] E. Bjornson, M. Matthaiou, and M. Debbah, "A New Look at Dual-hop Relaying: Performance Limits with Hardware Impairments", *IEEE Transactions on Communications*, vol. 61, pp. 4512–4525, 2013 (https://doi.org/10.1109/TCOMM.2013.100913.130282).
[31] N.T. Anh *et al.*, "Reliability-security Analysis for Harvest-to-jam Based Multi-hop Cluster MIMO Networks Using Cooperative Jamming Methods Under Impact of Hardware Impairments", *EAI Endorsed Transactions on Industrial Networks and Intelligent Systems*, vol. 8, pp. 1–11, 2021 (https://doi.org/10.4108/eai.17-9-2021.170963).
[32] C. Dhote, A. Singh, and P.K. Sharma, "RIS Assisted Near Field Communication in Sub-6 GHz Band: Experimental Perspective", *IEEE Communications Letters*, vol. 29, pp. 1814–1818, 2025 (https://doi.org/10.1109/LCOMM.2025.3576503).
[33] L. Dai *et al.*, "Reconfigurable Intelligent Surface-based Wireless Communications: Antenna Design, Prototyping, and Experimental Results", *IEEE Access*, vol. 8, pp. 45913–45923, 2020 (https://doi.org/10.1109/ACCESS.2020.2977772).
[34] P.T. Tran, T.N. Nguyen, and L.T. Tu, *Developing MATLAB Comprehensive Simulation for 5G/6G Wireless Communications*, Springer Singapore, 2026 (ISBN 9789819511167).
[35] M.A. Badiu and J.P. Coon, "Communication Through a Large Reflecting Surface with Phase Errors", *IEEE Wireless Communications Letters*, vol. 9, pp. 184–188, 2020 (https://doi.org/10.1109/LWC.2019.2947445).

Lam-Thanh Tu, Ph.D.
Communication and Signal Processing Research Group
Faculty of Electrical and Electronics Engineering
https://orcid.org/0000-0001-5735-4641
E-mail: tulamthanh@tdtu.edu.vn
Ton Duc Thang University, Ho Chi Minh City, Vietnam
https://tdtu.edu.vn

Bui Vu Minh, M.Sc.
Faculty of Engineering and Technology
https://orcid.org/0000-0003-0222-166X
E-mail: bvminh@ntt.edu.vn
Nguyen Tat Thanh University, Ho Chi Minh City, Vietnam
https://ntt.edu.vn

Tan N. Nguyen, Ph.D.
Advanced Intelligent Technology Research Group
Faculty of Electrical and Electronics Engineering
https://orcid.org/0000-0002-2286-6652
E-mail: nguyennhattan@tdtu.edu.vn
Ton Duc Thang University, Ho Chi Minh City, Vietnam
https://tdtu.edu.vn